



# Improved ozone simulation in East Asia via assimilating observations from the first geostationary air-quality monitoring satellite: Insights from an Observing System Simulation Experiment

Lei Shu<sup>a</sup>, Lei Zhu<sup>a,b,\*</sup>, Juseon Bak<sup>c</sup>, Peter Zoogman<sup>d</sup>, Han Han<sup>e</sup>, Xin Long<sup>a</sup>, Bin Bai<sup>a</sup>, Song Liu<sup>a</sup>, Dakang Wang<sup>a</sup>, Wenfu Sun<sup>a</sup>, Dongchuan Pu<sup>a</sup>, Yuyang Chen<sup>a</sup>, Xicheng Li<sup>a</sup>, Shuai Sun<sup>a</sup>, Juan Li<sup>a</sup>, Xiaoxing Zuo<sup>a</sup>, Xin Yang<sup>a,b</sup>, Tzung-May Fu<sup>a,b</sup>

<sup>a</sup> School of Environmental Science and Engineering, Southern University of Science and Technology, Shenzhen, Guangdong, 518055, China

<sup>b</sup> Guangdong Provincial Observation and Research Station for Coastal Atmosphere and Climate of the Greater Bay Area, Shenzhen, Guangdong, 518055, China

<sup>c</sup> Institute of Environmental Studies, Pusan National University, Busan, 46241, Republic of Korea

<sup>d</sup> Harvard-Smithsonian Center for Astrophysics, Cambridge, MA, 02138, United States

<sup>e</sup> Department of Atmospheric and Oceanic Sciences, School of Physics, Peking University, Beijing, 100871, China

## HIGHLIGHTS

- An OSSE is configured using two independent chemical transport models.
- The benefit of GEMS geostationary satellite observations is evaluated.
- Assimilating GEMS data improves near-surface ozone simulation in urban areas.
- Improvement in the middle to upper tropospheric ozone simulation is achieved.

## ARTICLE INFO

### Keywords:

Ozone  
GEMS  
OSSE  
Data assimilation

## ABSTRACT

The Geostationary Environment Monitoring Spectrometer (GEMS) is the world's first air quality instrument in the geostationary (GEO) orbit to monitor trace gases and aerosols at an unprecedented spatial and temporal resolution over East Asia, shedding light on the gradually alarming ozone pollution contrary to declining precursor emissions in this region. Here we use synthetic GEMS ozone profiles through the Observing System Simulation Experiment (OSSE) for evaluating the benefit of GEMS hourly measurements on chemical data simulation based on a Kalman filter technique. Assimilating synthetic GEMS data improves surface ozone simulation as its root-mean-square error (RMSE) is reduced by 7.2–19.2% over major urban areas in East Asia, along with a more accurate (6.3–29.2%) capturing of high-ozone events. The assimilation also better represents ozone vertical distributions in the middle to upper troposphere and better captures stratospheric intrusion events, with an RMSE reduction of 18.2–49.2% between 200 and 300 hPa. Our OSSE study offers a valuable reference for future ozone simulations, especially when massive observations become available in the coming era of GEO satellites.

## 1. Introduction

Ozone pollution is alarming in the populous East and Southeast Asia (Chang et al., 2017; Lu et al., 2018; Ziemke et al., 2019), posing significant threats to public health and the ecosystem (Monks et al., 2015; Yue et al., 2017). Optional ozone observations in this region, however,

remain inadequate, even non-existent in some areas, thus preventing the community from fully understanding and effectively mitigating its ozone pollution. As the world's first geostationary (GEO) air quality monitoring satellite instrument, the Geostationary Environment Monitoring Spectrometer (GEMS) (Kim et al., 2020) offers unprecedented opportunities to fill the observational gaps over this region with hourly

\* Corresponding author. School of Environmental Science and Engineering, Southern University of Science and Technology, Shenzhen, Guangdong, 518055, China.  
E-mail address: [zhul3@sustech.edu.cn](mailto:zhul3@sustech.edu.cn) (L. Zhu).

<https://doi.org/10.1016/j.atmosenv.2022.119003>

Received 21 November 2021; Received in revised form 27 January 2022; Accepted 12 February 2022

Available online 16 February 2022

1352-2310/© 2022 Elsevier Ltd. All rights reserved.

measurements of ozone and its precursors in the daytime. Here we demonstrate and quantify the benefit of GEMS hourly observations on improving ozone simulations in East and Southeast Asia through the Observing System Simulation Experiment (OSSE) (Timmermans et al., 2015; Claeysman et al., 2011; Zoogman et al., 2011, 2014a, 2014b; Quesada-Ruiz et al., 2020), setting the stage for future applications of GEO observations for air quality management.

East and Southeast Asia have been facing a worsening ozone problem in the last decade (Chen et al., 2021). Observations from the surface network reveal a steady increase ( $\sim 4\text{--}8\%$   $\text{yr}^{-1}$ ) in daily maximum 8-h average (MDA8) ozone concentrations in China (Han et al., 2020; Dang et al., 2021; D. Gao et al., 2021), along with more frequent high-ozone events from 2013 to 2020 (Gong et al., 2020; Shu et al., 2016, 2020). Nationwide, Chinese summertime MDA8 ozone ramps up at a rate of  $5\%$   $\text{yr}^{-1}$  from 2013 to 2019 (Lu et al., 2020). In South Korea, the annual mean surface ozone increases in all administrative districts from 2001 to 2018 (by  $0.3\text{--}1.7$  ppbv  $\text{yr}^{-1}$ ) (Yeo et al., 2021). Previous studies also reported the elevated MDA8 ozone exceeding 50 ppbv over the Indo-chinese peninsula and downstream areas due to biomass burning (Yadav et al., 2017; Marvin et al., 2021).

Chemical transport models (CTMs) have been widely used to understand non-linear ozone chemistry. But applications in Asia conclude that various factors, such as meteorological fields, chemical initial and boundary conditions, emission inventories, or chemical mechanisms, could all potentially lead to biased ozone simulations (M. Gao et al., 2020; J. Li et al., 2019; Shu et al., 2020). For example, the modeled annual mean surface ozone from 14 state-of-the-art CTMs within the framework of the Model Inter-Comparison Study for Asia Phase III (MICS-Asia III) is biased by  $-0.5$  to  $1.2$  ppbv in the North China Plain,  $-0.6$  to  $0.7$  ppbv in the Pearl River Delta, and  $-0.3$  to  $0.3$  ppbv in the northwestern Pacific and Japan (J. Li et al., 2019).

Data assimilation is an effective tool to improve the simulations of surface and tropospheric ozone (Bocquet et al., 2015; Wu et al., 2008; Huang et al., 2015; Miyazaki et al., 2012, 2020; Parrington et al., 2008, 2009; Inness et al., 2015, 2019), as well as the forecasting of surface ozone (Tang et al., 2011; Peng et al., 2018; Ma et al., 2019). These assimilation applications largely utilize the spatially and temporally continuous observations from the low Earth orbit (LEO) (Huang et al., 2015; Miyazaki et al., 2012, 2020; Inness et al., 2015, 2019), such as Ozone Monitoring Instrument (OMI) (Levelt et al., 2018) and TROPospheric Monitoring Instrument (TROPOMI) (Veefkind et al., 2012). For example, assimilation of LEO satellite observations results in a root-mean-square error (RMSE) reduction of 34–54% at the surface (Zoogman et al., 2011), an absolute bias reduction of  $\sim 25\text{--}30\%$  in the mid-troposphere (Parrington et al., 2008), and a reduced bias from 30–40% to  $< 10\%$  in the middle and upper troposphere (Miyazaki et al., 2012).

Monitoring air quality from space is entering a new era of GEO satellites with the capabilities of observing the diurnal variations of trace gases and aerosols for the first time. A virtual GEO constellation, consisting of GEMS (over Asia), Tropospheric Emissions: Monitoring of Pollution (TEMPO; North America) (Zoogman et al., 2017), and Sentinel-4 (Europe) (Ingmann et al., 2012), would facilitate air quality monitoring over the major polluted and industrialized regions of the Northern Hemisphere, enabling a massive flow of observations for air quality applications, including data assimilation.

OSSE is a practical tool for evaluating the potential of proposed ozone observations from a new instrument to be added to an existing observing system, which has been applied to TEMPO (Zoogman et al., 2014a, 2014b) and Sentinel-4 (Quesada-Ruiz et al., 2020). Zoogman et al. (2014a) demonstrated the improved monitoring capability of ozone exceedances in the United States Intermountain West through assimilating TEMPO measurements - capturing 82% of the spatial distribution of high-ozone events. Quesada-Ruiz et al. (2020) similarly reported the added value of the Sentinel-4 observations on tropospheric ozone over Europe, suggesting an RMSE reduction of up to 20% in the

middle to upper troposphere. Bak et al. (2013, 2019) demonstrated that GEMS could measure tropospheric ozone with an accuracy comparable to OMI, but stratospheric ozone with slightly worse performance than OMI due to the insufficient spectral information below  $\sim 300$  nm. Here we demonstrate and quantify the improvement in surface and tropospheric ozone simulation in East Asia via assimilating GEMS hourly ozone profile observations with the OSSE approach and two independent CTMs, as described below.

## 2. Observing System Simulation Experiment (OSSE)

Fig. 1 outlines our OSSE framework that mainly involves the following steps. (1) In the *nature run*, we use the Weather Research and Forecasting model coupled with Chemistry (WRF-Chem) (Grell et al., 2005) to construct the “true” atmosphere. Here we select August 2019 as the study period to represent summertime ozone pollution in Asia. (2) We sample the “true” atmosphere according to GEMS’s schedule (01–08 UTC used in this study) and retrieve hourly ozone profiles (denoted as synthetic GEMS observations) following an optimal estimation (OE) algorithm (Rodgers, 2000). (3) In the *control run*, we use an independent global CTM GEOS-Chem (Bey et al., 2001; Park et al., 2004; Mao et al., 2013) to generate *a priori* ozone estimates. The independence of two different CTMs in various aspects (Sections 2.1 and 2.3) ensures the robustness of the OSSE. (4) Finally, in the *assimilation run*, we assimilate the synthetic GEMS observations into GEOS-Chem to obtain the optimal (*a posteriori*) estimates. By comparing paired differences between these two simulations (*control* and *assimilation run*) and the “true” atmosphere, we quantify the benefit of knowledge contributed by GEMS observations. The following sections provide details in each step.

### 2.1. Constructing the “true” atmosphere

To generate the “true” atmosphere, we use the WRF-Chem model (version 4.1), which has been previously applied in reproducing summertime ozone pollution in Asia (M. Gao et al., 2020; J. Li et al., 2019). We adopt a two-nested modeling domain (centered at  $35^{\circ}\text{N}$ ,  $103^{\circ}\text{E}$ ) covering most of East Asia ( $60\text{ km} \times 60\text{ km}$ , not shown) with a nested grid resolution of  $20\text{ km} \times 20\text{ km}$  (shown in Fig. 2) and 34 vertical layers extending from the surface to 50 hPa. The meteorological initial and

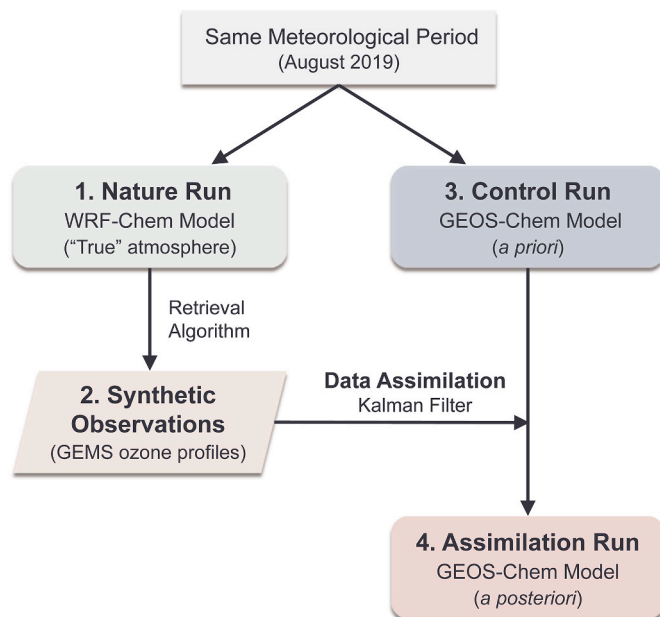
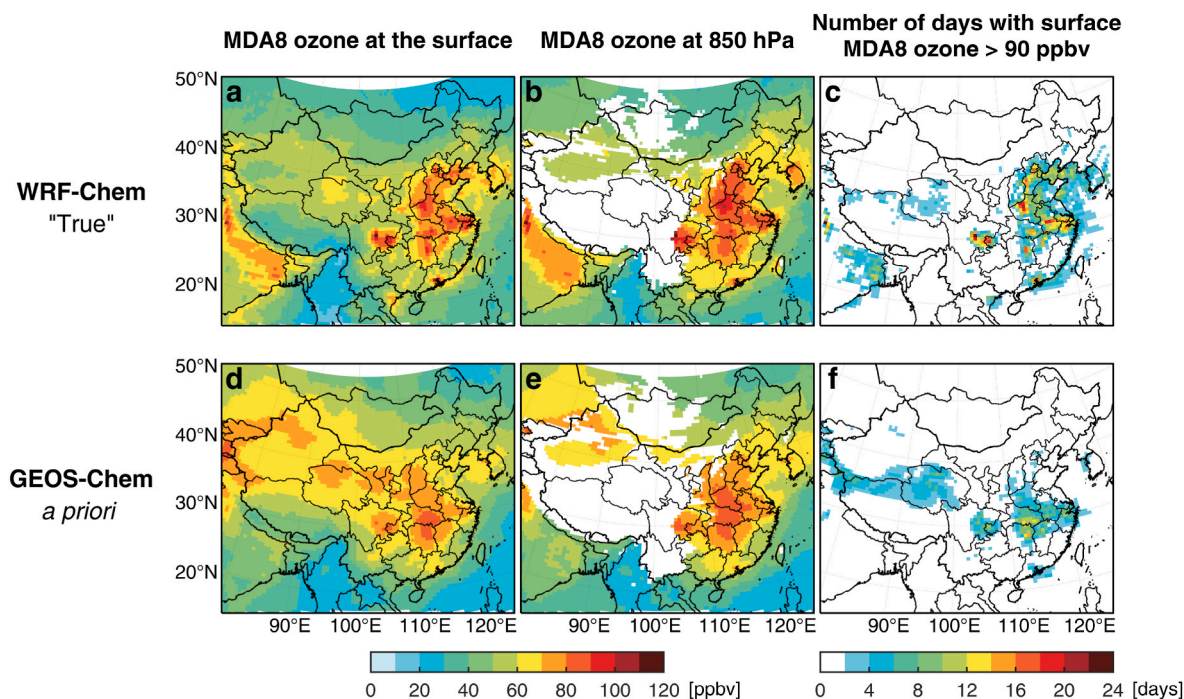


Fig. 1. Flowchart of the Observing System Simulation Experiment (OSSE) for assimilation of GEMS hourly ozone profile observations. Modified from Brasseur and Jacob (2017).



**Fig. 2.** Monthly mean values of the daily maximum 8-h average (MDA8) ozone at the surface (a, d) and 850 hPa (b, e), and the number of high-ozone events (defined as surface MDA8 ozone exceeding 90 ppbv; c, f) in August 2019. The top panels are from the “true” atmosphere constructed with WRF-Chem in the *nature run* (Section 2.1). The bottom panels show the *a priori* estimates from the GEOS-Chem *control run* (Section 2.3). WRF-Chem outputs are regridded onto the  $0.5^\circ \times 0.625^\circ$  GEOS-Chem grids.

boundary conditions are from the National Centers for Environmental Prediction (NCEP) Final (FNL) operational global analysis (<https://rda.ucar.edu/datasets/ds083.3>) with a temporal resolution of 6 h and a spatial resolution of  $0.25^\circ \times 0.25^\circ$ . The chemical initial and boundary conditions are from the Whole Atmosphere Community Climate Model (WACCM) (Gettelman et al., 2019) model 6 h outputs (<https://www.acom.ucar.edu/waccm/download.shtml>).

Emissions in the *nature run* are from state-of-the-art inventories. Specifically, anthropogenic emissions within China are prepared using the  $0.25^\circ \times 0.25^\circ$  Multi-resolution Emission Inventory for China (MEIC; <http://www.meicmodel.org>) (Zheng et al., 2018) in 2016 and scaled to the simulation year of 2019 according to their relative changes since 2013. Outside China, the associated emissions are from the Emissions Database for Global Atmospheric Research-Hemispheric Transport of Air Pollution (EDGAR-HTAP) (Janssens-Maenhout et al., 2015) for the year of 2010 at the  $0.1^\circ \times 0.1^\circ$  resolution. Biogenic emissions are calculated online using the Model of Emissions of Gases and Aerosols from Nature (MEGAN) (Guenther et al., 2012). Fire emissions are from Fire INventory from NCAR (FINN) version 1.5 (Wiedinmyer et al., 2011). We select the CBMZ chemical mechanism (Zaveri et al., 1999) for gas-phase chemistry and the MOSAIC aerosol scheme configured with 4 sectional aerosol bins (Zaveri et al., 2008). The simulation period spans from 29 July to 31 August 2019, with a spin-up time of 64 h and a temporal resolution of 1 h.

Comparing with surface observations over China indicates that the “true” atmosphere from the *nature run* reproduces the spatial distribution of observed MDA8 ozone concentrations in August 2019, with a spatial correlation coefficient ( $r$ ) of 0.82 and a mean bias of +6.5 ppbv (relative bias of +11.3%) over 337 cities (Fig. S1). The “true” atmosphere shows elevated MDA8 ozone and frequent high-ozone events (here and elsewhere defined as surface MDA8 ozone exceeding 90 ppbv) over regions with intensive anthropogenic emissions (Fig. 2a–c), such as eastern China and the Sichuan Basin (SCB). Fig. S2 further illustrates the overall consistency between simulated surface ozone with hourly observations in terms of temporal variations, as well as between simulated

ozone profiles with ozonesonde measurements. As such, we conclude that the “true” atmosphere is representative of the real atmosphere, at least to a large degree, with realistic model errors dedicated to the robustness of the OSSE.

## 2.2. Synthetic GEMS observations

The GEMS instrument is an ultraviolet (UV) and visible (Vis) imaging spectrometer onboard the Geostationary Korea Multi-Purpose satellite (Geo-KOMPSAT)-2B launched on 18 February 2020. It collects hourly daytime measurements of ozone, nitrogen dioxide, sulfur dioxide, formaldehyde, and aerosols over East Asia ( $5^\circ\text{S}$ – $45^\circ\text{N}$  in latitude and  $75^\circ$ – $145^\circ\text{E}$  in longitude) with a temporal resolution of 8 times per day (at least) and a spatial resolution of  $7 \times 8 \text{ km}^2$  (at Seoul).

Since GEMS science data products are not released yet, here ozone profiles for the daytime period (01–08 UTC) are simulated from GEMS synthetic measurements with a similar approach to the GEMS standard ozone profile algorithm (Bak et al., 2013, 2021) based on the OE method (Rodgers, 2000). In this experiment, the OE problem is linearly formulated as follows without doing actual iterative non-linear retrievals.

$$\hat{x} = x_{ap} + A(x_t - x_{ap}) + \hat{\varepsilon} \quad (1)$$

where

$$A = (K^T S_y^{-1} K + S_a^{-1})^{-1} K^T S_y^{-1} K = \hat{S} K^T S_y^{-1} K = G K \quad (2)$$

$$\hat{\varepsilon} = G \varepsilon_y \quad (3)$$

The retrieval of  $x$  ( $\hat{x}$ ) is considered as a linear combination of the true state ( $x_t$ , from WRF-Chem outputs) and *a priori* ( $x_{ap}$ ), weighted by the measurement error covariance matrix  $S_y$  and the *a priori* error covariance matrix  $S_a$ . The averaging kernel matrix  $A \equiv \partial \hat{x} / \partial x_t$ , used as a weighting term, represents the sensitivity of retrievals to the “true” atmosphere.  $G \equiv \partial \hat{x} / \partial y$  describes the sensitivity of retrievals to radiances ( $y$ ), while  $K \equiv \partial y / \partial x_t$  is the sensitivity of radiances to the “true”

atmosphere. Each diagonal element of  $A$  is a degree of freedom for signal (DFS), quantifying the number of independent pieces of information available at that layer from radiance measurements.  $(A-I)(x_t - x_{ap})$  and  $\hat{\varepsilon}$  represent the smoothing error and random-noise error, respectively.  $I$  is the identity matrix. The root sum square of these two retrieval errors represents the solution error ( $\sqrt{\hat{S}}$ ).

The state vector consists of the ozone profiles at 24 layers, surface albedo, and cloud fraction. The pressure level grid is set at  $P_i = 2^{-\frac{i}{23}} atm$  for  $i = 0$  to 23 ( $1 atm = 1013.25 hPa$ ) and with the top of the atmosphere set for  $P_{24}$  ( $\sim 65 km$ ), resulting in  $\sim 2.5 km$ -thick for each layer. To complete the “true” ozone profiles, WRF-Chem-based “true” atmosphere (Section 2.1) is exploited and extended with GEOS-Chem outputs (Section 2.3) above  $\sim 50 hPa$  due to the top pressure limit of the WRF-Chem simulations and then are spatially and temporally nested onto the GEMS full central scan scenario according to Kim et al. (2020). Moreover, the native spatial resolution is downgraded by  $4 \times 4$  binning, in line with the GEMS science data processing plan to reduce measurement noise and computational budget.

The surface albedo is defined based on the Earth surface reflectivity climatology at 347 nm from OMI data (Kleipool et al., 2008). Ozone *a priori* state vector ( $x_{ap}$ ) and corresponding error covariance matrix ( $S_a$ ) are taken from the climatological dataset of monthly zonal mean ozone profiles (McPeters and Labow, 2012).  $\hat{\varepsilon}$  is comprised of the retrieval errors due to measurement random-noise errors simulated through the GEMS signal-to-noise model developed by Ball aerospace.

The weighting functions of radiance observations with respect to elements in the state vector are simulated to define  $A$  and  $G$  matrices. The GEMS observations include ultraviolet and visible wavelengths from 300 to 500 nm with 0.2 nm spectral sampling and about 0.6 nm full-

width at half-maximum (FWHM) resolution. The spectral range of 300–340 nm is targeted for ozone profile retrievals, and hence 200 individual wavelengths are required to be simulated per one pixel. A lookup-table approach is employed to simulate GEMS spectra to reduce the computational cost. The version 2.8 Vector Linearized Discrete Ordinate Radiative Transfer (VLIDORT) (Spurr, 2006) model is used as the radiative transfer model. We followed the recipe introduced in Bak et al. (2021) to create the lookup tables, except that the high-resolution input spectra (ozone cross-section, Rayleigh scattering coefficient, and solar reference spectrum) is convolved with the GEMS slit function assumed to be the standard Gaussian before running the radiative transfer model.

The averaging kernels and retrieval errors are shown in Fig. S3 to characterize the GEMS ozone profile retrieval. It illustrates that GEMS provides no measurement information for the upper atmospheric layers above  $\sim 2 hPa$  (DFS is close to zero), and hence retrievals are almost determined by the *a priori* information. However, the retrieval quality is significantly better than *a priori* information for representing the stratosphere and troposphere, with the DFS value of 0.2–0.3 at each layer, providing sufficient information to resolve the ozone layer in the middle stratosphere. On the other hand, the tropospheric ozone variability is significantly smoothed out.

Nevertheless, the capabilities of GEMS in sensing the hot spots of ozone pollution over Northeast Asia and its chemical evolution are promising, as seen from Fig. 3, where GEMS retrievals at the surface layer are mapped on 16 August 2019 for 02, 04, 06, and 08 UTC, respectively. Fig. 4 compares the diurnal changes of monthly ground-level ozone between GEMS and the “true” atmosphere for August, but at three selected cities with high ozone concentrations (Fig. 3). It illustrates a better retrieval sensitivity at local time noon and lower latitude

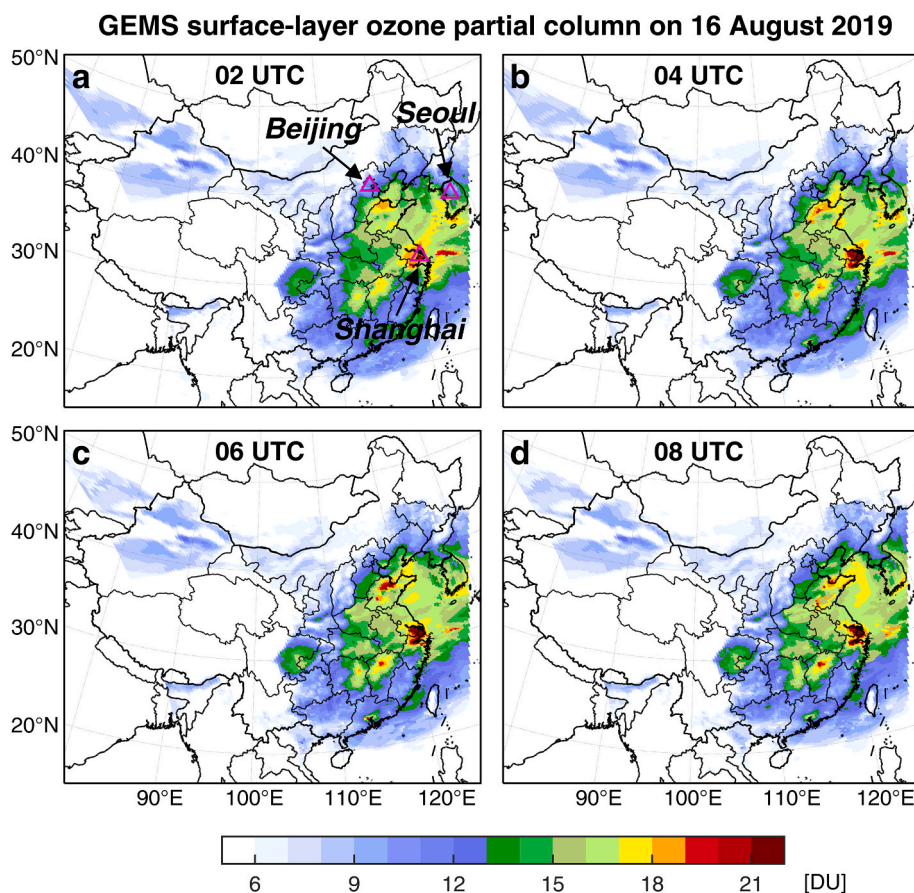


**Fig. 3.** GEMS surface-layer ozone partial column throughout the day (02, 04, 06, and 08 UTC) on 16 August 2019. The hollow triangles show the locations of Beijing (40.1°N, 116.2°E), Shanghai (31.3°N, 121.3°E), and Seoul (37.0°N, 127.5°E).

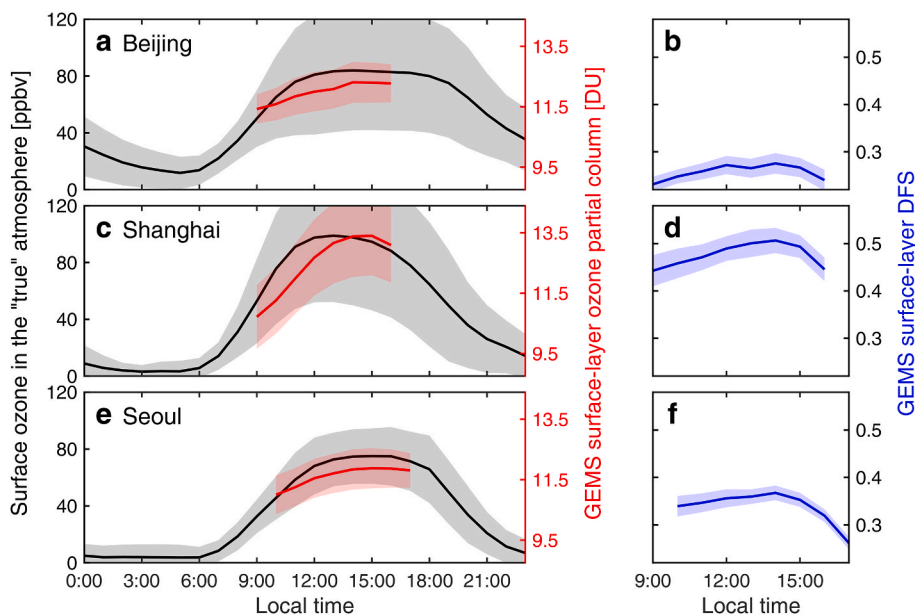


**Fig. 4.** Diurnal variations in monthly mean WRF-Chem-simulated surface ozone (black; referred as the “true” atmosphere; Section 2.1), GEMS surface-layer ozone partial column (red), and the corresponding degree of freedom for signal (DFS, defined as the trace of the averaging kernel matrix, Section 2.2; blue) at Beijing, Shanghai, and Seoul in August 2019. Black (red/blue) shaded area denotes 1.0 (0.25) standard deviation. (For interpretation of the references to colour in this figure legend, the reader is referred to the Web version of this article.)

where solar zenith angle reaches its minimum value. GEMS observations generally match well with the “true” atmosphere at three cities, while the DFS values are much higher at Shanghai (Fig. 4b,d,f). We attribute this to the impact of *a priori* information on OE-based retrievals. The climatological *a priori* ozone value is  $\sim 10$  DU at the surface layer, significantly lower than the “true” values, leading to significant retrieval biases at Shanghai (Fig. S3).

### 2.3. Control run with GEOS-Chem

We use a nested version of the GEOS-Chem (version 12.9.3; <http://www.geos-chem.org>) as the forward model in data assimilation. GEOS-Chem is a global 3-D CTM with a detailed  $\text{HO}_x$ - $\text{NO}_x$ -VOC-ozone-aerosol-halogen tropospheric chemistry mechanism (Bey et al., 2001; Park et al., 2004; Mao et al., 2013) and has been widely applied in ozone simulations (Zoogman et al., 2014a; Dang et al., 2021; Gong et al., 2020). The nested simulation over Asia ( $11^\circ\text{S}$ – $55^\circ\text{N}$ ,  $60^\circ$ – $150^\circ\text{E}$ ) is at a resolution of  $0.5^\circ \times 0.625^\circ$  with 47 vertical layers up to 0.1 hPa and boundary conditions updated every 3 h from a global  $2^\circ \times 2.5^\circ$  simulation. The global and nested simulations have a respective spin-up time of 1 year and 3 months, both driven by Modern-Era Retrospective Analysis for Research and Applications, Version 2 (MERRA-2) meteorological fields (Gelaro et al., 2017). Global anthropogenic emissions are from the Community Emissions Data System (CEDS) (Hoesly et al., 2018), substituted by MIX inventory (M. Li et al., 2017) over Asia. Biogenic emissions are calculated online using MEGAN (Guenther et al., 2012). Biomass burning emissions are from the fourth-generation Global Fire Emissions Database (GFED4) (Giglio et al., 2013).

Compared with WRF-Chem simulations (Section 2.1), here we configure GEOS-Chem as differently as possible in meteorological fields, chemical mechanisms, and emission inventories to maximize its independence, which is critical for the proper interpretation of OSSE results as previously stated. Fig. 2d,e shows the *a priori* near-surface MDA8 ozone from the *control run*, which is generally lower than the “true” atmosphere in urban areas (Fig. 2a,b). Such a discrepancy is even profound in major polluted urban agglomerations, including Beijing-Tianjin-Hebei (BTH), Yangtze River Delta (YRD), Pearl River Delta (PRD), and SCB regions in China, as well as the Seoul metropolitan area in South Korea, the Hanoi metropolitan area in Vietnam, and the Vientiane metropolitan area in Laos. In addition, the differences in monitoring high-ozone events are also substantial between the

simulations from two differently-configured models (Fig. 2c,f). In the free troposphere, ozone from the *control run* differs from that in the “true” atmosphere (Fig. S4), although both simulations produce similar spatial patterns. In the lower troposphere (700 hPa; Fig. S4a,d), we see higher ozone from the *control run* over most of the domain. In the upper troposphere (200 hPa; Fig. S4c,f), we find exceptionally higher ozone in regions north of China from the *nature run*, which may be associated with transboundary transport. In summary, the differences in spatial and vertical ozone distributions between *control run* and *nature run* highlight a well-designed yet challenging OSSE.

### 2.4. Assimilation run with GEOS-Chem

In the *assimilation run*, we adopt a sequential sub-optimal Kalman filter technique, as previously applied in TEMPO (Zoogman et al., 2014a, 2014b) and Tropospheric Emission Spectrometer (TES) (Parrington et al., 2008, 2009) ozone data assimilation. The daytime (01–08 UTC) synthetic GEMS observations are assimilated at successive 1 h time steps. At each assimilation time step, we calculate the optimal profile  $\hat{x}^a$  as a weighted average of the model forecast  $x^b$  and the observation  $\hat{x}^{obs}$  (from Section 2.2).

$$\hat{x}^a = x^b + M(\hat{x}^{obs} - Hx^b) \quad (4)$$

where  $H$  is the observation operator that maps the higher resolution model profile into the retrieval space. This operator uses the spatial interpolation operator  $S$ , as well as the *a priori* profile  $x_{ap}$  and averaging kernels  $A$  from GEMS retrievals (Section 2.2). This procedure removes the dependence of the analysis on the model-retrieval comparison (Miyazaki et al., 2012, 2020). Different from some air quality OSSEs reviewed by Timmermans et al. (2015), a distinct feature of our work is the use of space- and time-varying averaging kernels.

$$Hx^b = x_{ap} + A(Sx^b - x_{ap}) \quad (5)$$

We limit our assimilation exercise to GEMS pixels with cloud fraction less than 0.3 and only utilize GEMS ozone profiles at 11 retrieval layers from the surface to  $\sim 26.6$  hPa in our assimilation to avoid introducing redundant stratospheric information. The Kalman gain matrix  $M$  (denoted as  $M$  to avoid confusion relative to Section 2.2) measures the relative weight given to the model and the observation:

$$M = P^b H^T (H P^b H^T + R)^{-1} \quad (6)$$

where  $P^b$  is the background error covariance matrix, and  $R$  is the observation error covariance matrix provided with the GEMS retrieval (assumed diagonal).

The observation error (*i.e.*, solution error; Section 2.2) is reduced by the square root of the number of observations averaged over each GEOS-Chem grid square following Zoogman et al. (2014a). We assume zero representation error since the synthetic GEMS observations are spatially dense compared with GEOS-Chem. The analysis error covariance matrix is calculated as:

$$P^a = (I - MH)P^b \quad (7)$$

where  $I$  is the identity matrix. Following Zoogman et al. (2011), we use the square of 25% of the background profile to initialize the model error variances (diagonal terms of  $P^b$ ). Concerning the off-diagonal terms, we parameterize the model error covariances by a vertical error correlation length of 1.7 km (Fig. S5) and neglect horizontal correlations, which could constrain the spreading of the information from GEMS retrievals and make the current assimilation setup suboptimal (Parrington et al., 2008). To make the computation tractable in the assimilation, we solve Eq. (4) column by column following Zoogman et al. (2014a).

### 3. Benefit of assimilating GEMS observations on ozone simulations

#### 3.1. Improved simulations of near-surface ozone

We quantify the added value from GEMS observations on simulating near-surface ozone by comparing the *a priori* (without assimilation, *control run*) and *a posteriori* (with assimilation of GEMS observations, *assimilation run*) from GEOS-Chem simulations to the “true” atmosphere (*nature run*).

As displayed in Fig. 5, assimilation of GEMS hourly ozone observations improves the model performance by reducing biases in both mean near-surface ozone and days of high-ozone events. Before assimilation, the *a priori* ozone at the surface is biased low in urban agglomerations with respect to the *nature run* with a mean bias ranging from  $-15.9$  to  $-2.3$  ppbv (Fig. 5a). After assimilation, we see lower biases and reduced RMSE (by 7.2–19.2%) in surface ozone over the same regions, with more distinct improvement observed in YRD and Hanoi where RMSE being reduced by  $\sim 20\%$  (Fig. 5d). In addition, assimilating GEMS observations leads to a 0.2–1.4 days (6.3–29.2%) improvement in capturing high-ozone events, with the most significant improvement in YRD (29.2%) and SCB (20.3%) (Fig. 5c,f). Within the boundary layer, assimilation of GEMS observations provides practical constraints on ozone as well (Fig. 5b,e). At 850 hPa, the RMSE of ozone bias is reduced by 0.4–3.9 ppbv (7.1–31.4%) after assimilation, comparable to the improvement achieved at the surface. In western China, however, assimilating GEMS data fails to introduce much improvement. We attribute this to the large positive bias in the *a priori* (Fig. 5a) and low retrieval sensitivity to surface ozone (Fig. S6). The slight overestimation of high-ozone days in southeast China (*e.g.*, Hunan, Hubei, and Jiangxi provinces), however, gets amplified after assimilation, which likely stems from the improper specification of model errors. This calls for assimilating in-situ observations to better constrain near-surface ozone.

We further examine the ability of the assimilation system to characterize the day-to-day ozone variations. Assimilating GEMS hourly observations is able to better characterize the variations in daily MDA8 ozone on both regional and urban scales (Table 1). The negative mean bias over eastern China decreases from  $-4.2$  ppbv to  $-0.4$  ppbv. In particular, the mean biases in daily ozone are reduced by 2.7–5.2 ppbv in major urban agglomerations (BTH, YRD, and PRD) in China. Comparable improvement is obtained in Seoul and Hanoi (3.0–3.3 ppbv). Furthermore, by applying the reduced-major-axis (RMA) regression, we

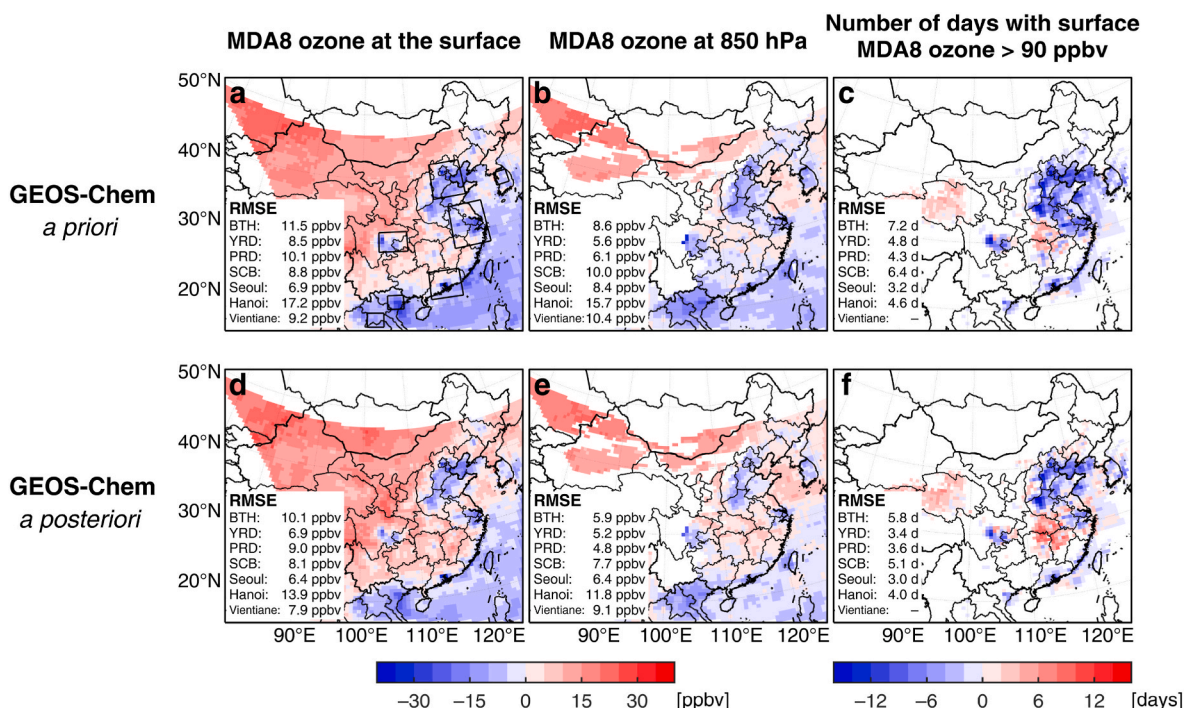


**Fig. 5.** Mean bias of the daily maximum 8-h average (MDA8) ozone at the surface (a, d) and 850 hPa (b, e), and the number of high-ozone events (defined as surface MDA8 ozone exceeding 90 ppbv; c, f) in August 2019 between the GEOS-Chem model and the WRF-Chem model (taken as the “true” atmosphere). The top (bottom) panels show the *a priori* (*a posteriori*) bias without (with) assimilation of GEMS observations across the GEMS full central scan scenario (Fig. 3). Polygons in (a) define the regions of the Beijing-Tianjin-Hebei (BTH: 36–41.5°N, 114–120°E), the Yangtze River Delta (YRD: 28–34.5°N, 116–122.5°E), the Pearl River Delta (PRD: 21–25°N, 111–116°E), the Sichuan Basin (SCB: 28.5–31.5°N, 103–108°E) in China, the Seoul metropolitan area in South Korea (Seoul: 36–38°N, 126–129°E), the Hanoi metropolitan area in Vietnam (Hanoi: 20–22°N, 104–107°E), and the Vientiane metropolitan area in Laos (Vientiane: 17.5–19.5°N, 101–104°E). Comparison statistics for these regions are given inset as the root-mean-square error (RMSE).

**Table 1**

Comparison statistics between the GEOS-Chem model and the WRF-Chem model (taken as the “true” atmosphere) in August 2019. The *a priori* (without assimilation, from the *control run*) and *a posteriori* (with assimilation of GEMS observations, from the *assimilation run*) surface daily maximum 8-h average (MDA8) ozone for all grid squares in given regions (defined in Fig. 5; eastern China: 20–42°N, 110–123°E) and for individual days are compared to the “true” atmosphere. Statistics include the mean bias and the slope of the reduced-major-axis regression line (the closer the slope to 1, the better agreement the *a priori*/*a posteriori* with “true” atmosphere). Also shown is the sample size (*N*).

Regions	<i>N</i>	Mean bias (ppbv)		Slope	
		<i>a priori</i>	<i>a posteriori</i>	<i>a priori</i>	<i>a posteriori</i>
Eastern China	30690	−4.2	−0.4	0.88	0.95
Beijing-Tianjin-Hebei	4092	−8.2	−5.5	0.60	0.76
Yangtze River Delta	4774	−5.4	−0.2	0.78	0.88
Pearl River Delta	2511	−4.9	−1.4	0.79	0.82
Sichuan Basin	1953	−2.3	1.1	0.77	0.75
Seoul metropolitan area	775	−3.3	−0.3	0.71	0.78
Hanoi metropolitan area	775	−15.9	−12.6	0.68	0.96
Vientiane metropolitan area	775	−8.9	−7.6	0.51	0.60

find that the *a posteriori* ozone estimates are consistently in better agreement with the “true” atmosphere for all the given regions (except for SCB) relative to the *a priori* estimates. Especially, the regression slope in Hanoi increases from 0.68 to 0.96, implying a substantial improvement in ozone simulation over this region. To conclude, these closer agreements confirm that the model errors are effectively reduced via assimilating GEMS observations.

We acknowledge that the above RMSE reduction (7.2–19.2%) in near-surface ozone simulation by assimilating GEMS data is less significant than assimilating in-situ observations (Tang et al., 2011; Ma et al., 2019). For example, Ma et al. (2019) indicated that the optimization of anthropogenic emissions and chemical initial conditions via assimilating surface multi-constituent observations is valuable for daytime ozone forecast as the RMSE is reduced by ~ 30%. However, the potential of geostationary ozone measurements from GEMS is still promising given

its unprecedented spatiotemporal resolution. More experiments are underway in the following work to figure out the added value of multi-platform data assimilation (e.g., GEMS and surface observations) dedicated to improved surface ozone simulations. Moreover, there is a gap between synthetic and actual observations since the GEMS science data products are still under development. Enhanced assimilation performance will be expected after conducting more strict quality control following the recommended data quality criteria in the coming GEMS ozone profile products.

### 3.2. Improved simulations of ozone vertical profiles

Next, we examine how assimilating GEMS ozone measurements improves the simulations of ozone vertical distributions, which plays a critical role in dominating the variations of ozone pollution near the

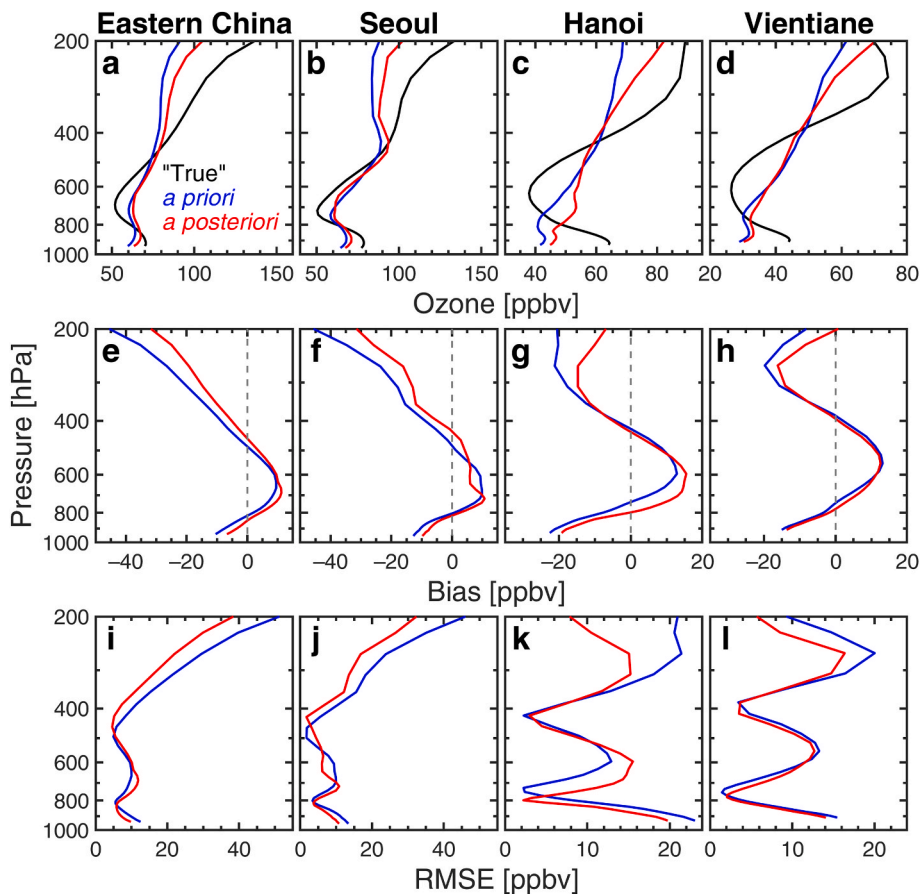


**Fig. 6.** Comparison of the vertical profiles of monthly mean daily maximum 8-h average (MDA8) ozone (a–d) between the *nature run* (“true”, black), *control run* (*a priori*, blue), and *assimilation run* (*a posteriori*, red) in August 2019 in eastern China, Seoul, Hanoi, and Vientiane (defined in Fig. 5 and Table 1). The middle (e–h) and bottom panels (i–l) show the bias and root-mean-square error (RMSE) between the *control* (*assimilation*) *run* and *nature run* in blue (red). (For interpretation of the references to colour in this figure legend, the reader is referred to the Web version of this article.)

surface by the transport from the free troposphere to the boundary layer. Since the added information through data assimilation of GEMS observations varies largely with space (Fig. 5), we limit the following analysis to eastern China, Seoul, Hanoi, and Vientiane.

Fig. 6 compares the ozone vertical profiles between the *nature run*, *control run*, and *assimilation run* in August 2019. At mid-latitudes (i.e., eastern China and Seoul), the *control run* shows a negative *a priori* bias near the surface (below 800 hPa) and in the middle to upper troposphere (200–500 hPa), while the forward model overestimates ozone concentrations in the lower to middle troposphere (500–800 hPa). After data assimilation, there is a clear reduction in ozone bias (by 25.6–31.7%) and RMSE (24.3–29.4%) in the middle to upper troposphere (200–300 hPa). Nevertheless, we see inadequate corrections made to modeling ozone in the lower to middle troposphere, as commonly revealed by Miyazaki et al. (2012) and Quesada-Ruiz et al. (2020). It indicates that GEMS ozone profile observations may not have enough information to sufficiently constrain the ozone vertical profiles owing to the low sensitivity and large observation errors (Fig. S3), as well as the sparse vertical gridding ( $\sim 2.5$  km-thick) in the troposphere, especially within the boundary layer (Section 2.2). Compared to mid-latitudes, at low latitudes (i.e., Hanoi and Vientiane) with a deeper troposphere layer, adding GEMS observations largely eliminates the negative bias in the middle to upper troposphere where RMSE being reduced by 18.2–49.2% between 200 and 300 hPa, leading to a closer agreement with the “true” atmosphere. In contrast, at the same time, a limited improvement is obtained for ozone profiles in the lower troposphere, as discussed above. It also suggests the need of multi-platform data assimilation (e.g., GEMS and ozonesonde measurements) to improve the assimilation performance.

The stratosphere-to-troposphere transport is thought to be the dominant source of tropospheric ozone (Monks et al., 2015; Han et al., 2019). We screen out a stratospheric intrusion event by scrutinizing the “true” atmosphere to evaluate how GEMS monitors ozone in terms of vertical distribution under such a condition. Fig. 7 provides a stratosphere-to-troposphere transport example along the longitude of 121.25°E on 15 August 2019. The stratospheric intrusion is characterized by a remarkable ligulate ozone enhancement extending to the lower troposphere (700 hPa) from high latitude to low latitude. The process is well-represented by the “true” atmosphere, whereas the GEOS-Chem model *a priori* similarly captures the stratospheric intrusion pattern but of a smaller magnitude in ozone concentrations. The *assimilation run*

shows the improved agreements with the “true” atmosphere relative to the *control run*. A substantial bias reduction is obtained between 200 and 500 hPa and between 600 and 800 hPa. There is an obvious time lag of the stratospheric intrusion event (18 UTC) with respect to the assimilation window (01–08 UTC), thus our results suggest that GEO measurements also provide valuable constraints on the diurnal variability in tropospheric ozone.

#### 4. Conclusions

We have performed an Observing System Simulation Experiment (OSSE) to evaluate how assimilating daytime hourly ozone observations from the Geostationary Environment Monitoring Spectrometer (GEMS) improves surface and tropospheric ozone simulations in East Asia. The OSSE utilizes the independence between two differently-configured models (GEOS-Chem and WRF-Chem), along with a Kalman filter technique. Assimilation of GEMS observations can potentially reduce biases in near-surface and middle to upper tropospheric ozone simulation, which would otherwise propagate freely without constraints. Specifically, the root-mean-square error (RMSE) of surface ozone bias is decreased by 7.2–19.2% after the assimilation over major Asian urban areas, resulting in a more accurate (6.3–29.2%) prediction of high-ozone events. The assimilation efforts also make noticeable adjustments in ozone vertical profiles in the middle to upper troposphere to better capture stratospheric intrusion events.

Our work offers a simulation reference for future ozone studies in East Asia, acknowledging uncertainties in the forward model, the assimilation technique, and synthetic GEMS observations may complicate the results. For example, an overestimation of errors in modeled ozone could lead to overoptimistic estimates of information contributed by GEMS (Zoogman et al., 2014a). Here the results of our study depend on the OSSE design and should be interpreted within the current observing system. Future assimilation exercises may want to pay attention to data screening by following data quality criteria in the coming GEMS ozone profile products. In addition, further investigation may benefit from additional constraints enabled by multi-spectral instruments (e.g., ultraviolet, infrared, or visible) or multi-platform (e.g., geostationary, low Earth orbit, ozonesonde, and ground-based stations) observations.

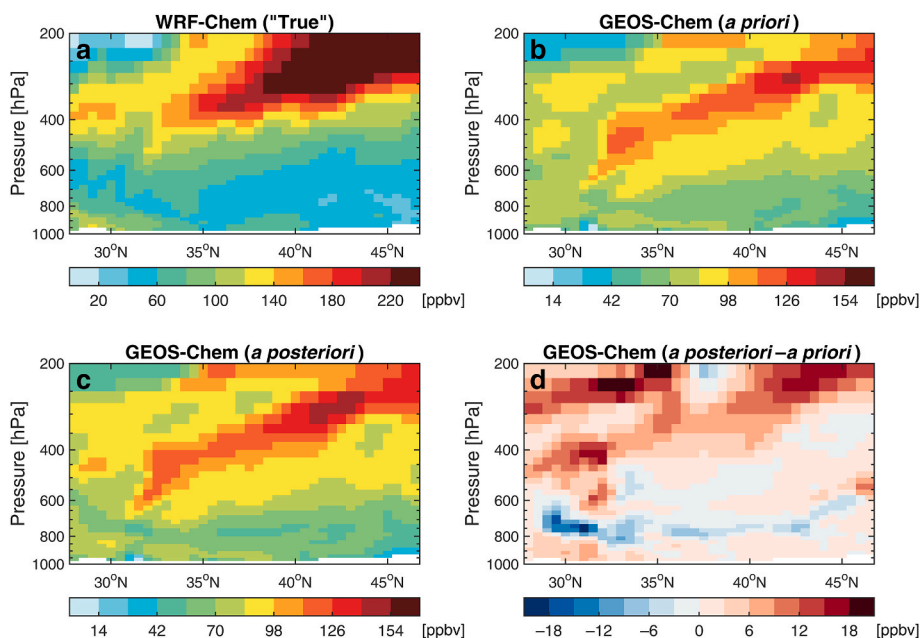


Fig. 7. Latitude-altitude cross-section of ozone concentrations (121.25°E, 18 UTC, on 15 August 2019). The “true” atmosphere constructed with WRF-Chem in the *nature run* (a) is compared to the *a priori* (without assimilation, from the *control run*; b) and *a posteriori* (with assimilation of GEMS observations, from the *assimilation run*; c) from the GEOS-Chem simulations. The bottom right panel (d) shows the difference between the *a posteriori* and the *a priori*. Note that the panel scales are different.

## CRediT authorship contribution statement

**Lei Shu:** Methodology, Software, Formal analysis, Writing – original draft, Writing – review & editing, Visualization, Funding acquisition. **Lei Zhu:** Conceptualization, Writing – original draft, Writing – review & editing, Supervision, Funding acquisition. **Juseon Bak:** Software, Writing – original draft, Writing – review & editing, Funding acquisition. **Peter Zoogman:** Methodology, Writing – review & editing. **Han Han:** Writing – review & editing. **Xin Long:** Software, Writing – review & editing. **Bin Bai:** Investigation. **Song Liu:** Resources. **Dakang Wang:** Resources. **Wenfu Sun:** Resources. **Dongchuan Pu:** Resources. **Yuyang Chen:** Resources. **Xicheng Li:** Resources. **Shuai Sun:** Resources. **Juan Li:** Resources. **Xiaoxing Zuo:** Resources. **Xin Yang:** Supervision. **Tzung-May Fu:** Supervision.

## Declaration of competing interest

The authors declare that they have no known competing financial interests or personal relationships that could have appeared to influence the work reported in this paper.

## Acknowledgements

This work is funded by the Key-Area Research and Development Program of Guangdong Province (2020B1111360001), Guangdong Basic and Applied Basic Research Foundation (2021A1515110713), Guangdong University Research Project Science Team (2021KCXTD004), Guangdong Basic and Applied Basic Research Fund Committee (2020B1515130003), Guangdong University Youth Innovation Talent Project (2020KQNCX066), Shenzhen Science and Technology Program (JCYJ20210324104604012), and China Postdoctoral Science Foundation (2021M701554). This work is supported by the Center for Computational Science and Engineering at Southern University of Science and Technology. Research at Pusan National University is supported by the Basic Science Research Program through the National Research Foundation of Korea (NRF) funded by the Ministry of Education (2020R1A6A1A03044834).

## Appendix A. Supplementary data

Supplementary data to this article can be found online at <https://doi.org/10.1016/j.atmosenv.2022.119003>.

## References

- Bak, J., Baek, K.H., Kim, J.H., Liu, X., Kim, J., Chance, K., 2019. Cross-evaluation of GEMS tropospheric ozone retrieval performance using OMI data and the use of an ozonesonde dataset over East Asia for validation. *Atmos. Meas. Tech.* 12 (9), 5201–5215. <https://doi.org/10.5194/amt-12-5201-2019>.
- Bak, J., Kim, J.H., Liu, X., Chance, K., Kim, J., 2013. Evaluation of ozone profile and tropospheric ozone retrievals from GEMS and OMI spectra. *Atmos. Meas. Tech.* 6 (2), 239–249. <https://doi.org/10.5194/amt-6-239-2013>.
- Bak, J., Liu, X., Spurr, R., Yang, K., Nowlan, C.R., Miller, C.C., et al., 2021. Radiative transfer acceleration based on the principal component analysis and lookup table of corrections: optimization and application to UV ozone profile retrievals. *Atmos. Meas. Tech.* 14 (4), 2659–2672. <https://doi.org/10.5194/amt-14-2659-2021>.
- Bey, I., Jacob, D.J., Yantosca, R.M., Logan, J.A., Field, B.D., Fiore, A.M., et al., 2001. Global modeling of tropospheric chemistry with assimilated meteorology: model description and evaluation. *J. Geophys. Res. Atmos.* 106 (D19), 23073–23095. <https://doi.org/10.1029/2001JD000807>.
- Bocquet, M., Elbern, H., Eskes, H., Hirtl, M., Žabkar, R., Carmichael, G.R., et al., 2015. Data assimilation in atmospheric chemistry models: current status and future prospects for coupled chemistry meteorology models. *Atmos. Chem. Phys.* 15 (10), 5325–5358. <https://doi.org/10.5194/acp-15-5325-2015>.
- Brasseur, G.P., Jacob, D.J., 2017. *Modeling of Atmospheric Chemistry*. Cambridge University Press, Cambridge. <https://doi.org/10.1017/9781316544754>.
- Chang, K.-L., Petropavlovskikh, I., Cooper, O.R., Schultz, M.G., Wang, T., 2017. Regional trend analysis of surface ozone observations from monitoring networks in eastern North America, Europe and East Asia. *Elementa: Science of the Anthropocene* 5, 50. <https://doi.org/10.1525/elementa.243>.
- Chen, X., Jiang, Z., Shen, Y., Li, R., Fu, Y., Liu, J., et al., 2021. Chinese regulations are working—why is surface ozone over industrialized areas still high? Applying lessons from northeast US air quality evolution. *Geophys. Res. Lett.* 48, e2021GL092816. <https://doi.org/10.1029/2021GL092816>.
- Claeyman, M., Attié, J.L., Peuch, V.H., El Amraoui, L., Lahoz, W.A., Josse, B., et al., 2011. A thermal infrared instrument onboard a geostationary platform for CO and O<sub>3</sub> measurements in the lowermost troposphere: observing System Simulation Experiments (OSSE). *Atmos. Meas. Tech.* 4 (8), 1637–1661. <https://doi.org/10.5194/amt-4-1637-2011>.
- Dang, R., Liao, H., Fu, Y., 2021. Quantifying the anthropogenic and meteorological influences on summertime surface ozone in China over 2012–2017. *Sci. Total Environ.* 754, 142394. <https://doi.org/10.1016/j.scitotenv.2020.142394>.
- Gao, D., Xie, M., Liu, J., Wang, T., Ma, C., Bai, H., et al., 2021. Ozone variability induced by synoptic weather patterns in warm seasons of 2014–2018 over the Yangtze River Delta region, China. *Atmos. Chem. Phys.* 21 (8), 5847–5864. <https://doi.org/10.5194/acp-21-5847-2021>.
- Gao, M., Gao, J., Zhu, B., Kumar, R., Lu, X., Song, S., et al., 2020. Ozone pollution over China and India: seasonality and sources. *Atmos. Chem. Phys.* 20 (7), 4399–4414. <https://doi.org/10.5194/acp-20-4399-2020>.
- Gelaro, R., McCarty, W., Suárez, M.J., Todling, R., Molod, A., Takacs, L., et al., 2017. The Modern-Era retrospective analysis for Research and applications, version 2 (MERRA-2). *J. Clim.* 30 (14), 5419–5454. <https://doi.org/10.1175/jcli-d-16-0758.1>.
- Gottelman, A., Mills, M.J., Kinnison, D.E., Garcia, R.R., Smith, A.K., Marsh, D.R., et al., 2019. The Whole atmosphere community climate model version 6 (WACCM6). *J. Geophys. Res. Atmos.* 124 (23), 12380–12403. <https://doi.org/10.1029/2019JD030943>.
- Giglio, L., Anderson, J.T., van der Werf, G.R., 2013. Analysis of daily, monthly, and annual burned area using the fourth-generation global fire emissions database (GFED4). *J. Geophys. Res.: Biogeosciences* 118 (1), 317–328. <https://doi.org/10.1002/jgrg.20042>.
- Gong, C., Liao, H., Zhang, L., Yue, X., Dang, R., Yang, Y., 2020. Persistent ozone pollution episodes in North China exacerbated by regional transport. *Environ. Pollut.* 265, 115056. <https://doi.org/10.1016/j.envpol.2020.115056>.
- Grell, G.A., Peckham, S.E., Schmitz, R., McKeen, S.A., Frost, G., Skamarock, W.C., Eder, B., 2005. Fully coupled “online” chemistry within the WRF model. *Atmos. Environ.* 39 (37), 6957–6975. <https://doi.org/10.1016/j.atmosenv.2005.04.027>.
- Guenther, A.B., Jiang, X., Heald, C.L., Sakulyanontvittaya, T., Duhl, T., Emmons, L.K., Wang, X., 2012. The Model of Emissions of Gases and Aerosols from Nature version 2.1 (MEGAN2.1): an extended and updated framework for modeling biogenic emissions. *Geosci. Model Dev. (GMD)* 5 (6), 1471–1492. <https://doi.org/10.5194/gmd-5-1471-2012>.
- Han, H., Liu, J., Shu, L., Wang, T., Yuan, H., 2020. Local and synoptic meteorological influences on daily variability in summertime surface ozone in eastern China. *Atmos. Chem. Phys.* 20 (1), 203–222. <https://doi.org/10.5194/acp-20-203-2020>.
- Han, H., Liu, J., Yuan, H., Wang, T., Zhuang, B., Zhang, X., 2019. Foreign influences on tropospheric ozone over East Asia through global atmospheric transport. *Atmos. Chem. Phys.* 19 (19), 12495–12514. <https://doi.org/10.5194/acp-19-12495-2019>.
- Hoesly, R.M., Smith, S.J., Feng, L., Klimont, Z., Janssens-Maenhout, G., Pitkanen, T., et al., 2018. Historical (1750–2014) anthropogenic emissions of reactive gases and aerosols from the Community Emissions Data System (CEDS). *Geosci. Model Dev. (GMD)* 11 (1), 369–408. <https://doi.org/10.5194/gmd-11-369-2018>.
- Huang, M., Bowman, K.W., Carmichael, G.R., Lee, M., Chai, T., Spak, S.N., et al., 2015. Improved western U.S. background ozone estimates via constraining nonlocal and local source contributions using Aura TES and OMI observations. *J. Geophys. Res. Atmos.* 120 (8), 3572–3592. <https://doi.org/10.1002/2014JD022993>.
- Ingmans, P., Veihelmann, B., Langen, J., Lamarre, D., Stark, H., Courrèges-Lacoste, G.B., 2012. Requirements for the GMES atmosphere service and ESA’s implementation concept: sentinels-4/-5 and -5p. *Remote Sens. Environ.* 120, 58–69. <https://doi.org/10.1016/j.rse.2012.01.023>.
- Inness, A., Blechschmidt, A.M., Bouarar, I., Chabrillat, S., Crepulja, M., Engelen, R.J., et al., 2015. Data assimilation of satellite-retrieved ozone, carbon monoxide and nitrogen dioxide with ECMWF’s Composition-IFS. *Atmos. Chem. Phys.* 15 (9), 5275–5303. <https://doi.org/10.5194/acp-15-5275-2015>.
- Inness, A., Flemming, J., Heue, K.P., Lerot, C., Loyola, D., Ribas, R., et al., 2019. Monitoring and assimilation tests with TROPOMI data in the CAMS system: near-real-time total column ozone. *Atmos. Chem. Phys.* 19 (6), 3939–3962. <https://doi.org/10.5194/acp-19-3939-2019>.
- Janssens-Maenhout, G., Crippa, M., Guizzardi, D., Dentener, F., Muntean, M., Pouliot, G., et al., 2015. HTAP\_v2.2: a mosaic of regional and global emission grid maps for 2008 and 2010 to study hemispheric transport of air pollution. *Atmos. Chem. Phys.* 15 (19), 11411–11432. <https://doi.org/10.5194/acp-15-11411-2015>.
- Kim, J., Jeong, U., Ahn, M.-H., Kim, J.H., Park, R.J., Lee, H., et al., 2020. new era of air quality monitoring from space: geostationary environment monitoring spectrometer (GEMS). *Bull. Am. Meteorol. Soc.* 101 (1), E1–E22. <https://doi.org/10.1175/bams-d-18-0013.1>.
- Kleipool, Q.L., Dobber, M.R., de Haan, J.F., Levelt, P.F., 2008. Earth surface reflectance climatology from 3 years of OMI data. *J. Geophys. Res. Atmos.* 113 (D18), D18308. <https://doi.org/10.1029/2008JD010290>.
- Levelt, P.F., Joiner, J., Tamminen, J., Veehkind, J.P., Bhartia, P.K., Stein Zweers, D.C., et al., 2018. The ozone monitoring instrument: overview of 14 years in space. *Atmos. Chem. Phys.* 18 (8), 5699–5745. <https://doi.org/10.5194/acp-18-5699-2018>.
- Li, J., Nagashima, T., Kong, L., Ge, B., Yamaji, K., Fu, J.S., et al., 2019. Model evaluation and intercomparison of surface-level ozone and relevant species in East Asia in the context of MICS-Asia Phase III – Part 1: Overview. *Atmos. Chem. Phys.* 19 (20), 12993–13015. <https://doi.org/10.5194/acp-19-12993-2019>.
- Li, M., Zhang, Q., Kurokawa, J.I., Woo, J.H., He, K., Lu, Z., et al., 2017. MIX: a mosaic Asian anthropogenic emission inventory under the international collaboration

- framework of the MICS-Asia and HTAP. *Atmos. Chem. Phys.* 17 (2), 935–963. <https://doi.org/10.5194/acp-17-935-2017>.
- Lu, X., Hong, J., Zhang, L., Cooper, O.R., Schultz, M.G., Xu, X., et al., 2018. Severe surface ozone pollution in China: a global perspective. *Environ. Sci. Technol. Lett.* 5 (8), 487–494. <https://doi.org/10.1021/acs.estlett.8b00366>.
- Lu, X., Zhang, L., Wang, X., Gao, M., Li, K., Zhang, Y., et al., 2020. Rapid increases in warm-season surface ozone and resulting health impact in China since 2013. *Environ. Sci. Technol. Lett.* 7 (4), 240–247. <https://doi.org/10.1021/acs.estlett.0c00171>.
- Ma, C., Wang, T., Mizzi, A.P., Anderson, J.L., Zhuang, B., Xie, M., Wu, R., 2019. Multiconstituent data assimilation with WRF-Chem/DART: potential for adjusting anthropogenic emissions and improving air quality forecasts over eastern China. *J. Geophys. Res. Atmos.* 124, 7393–7412. <https://doi.org/10.1029/2019JD030421>.
- Mao, J., Paulot, F., Jacob, D.J., Cohen, R.C., Crounse, J.D., Wennberg, P.O., et al., 2013. Ozone and organic nitrates over the eastern United States: sensitivity to isoprene chemistry. *J. Geophys. Res. Atmos.* 118 (19) <https://doi.org/10.1002/jgrd.50817>, 11,256–11,268.
- Marvin, M.R., Palmer, P.I., Latter, B.G., Siddans, R., Kerridge, B.J., Latif, M.T., Khan, M. F., 2021. Photochemical environment over Southeast Asia primed for hazardous ozone levels with influx of nitrogen oxides from seasonal biomass burning. *Atmos. Chem. Phys.* 21 (3), 1917–1935. <https://doi.org/10.5194/acp-21-1917-2021>.
- McPeters, R.D., Labow, G.J., 2012. Climatology 2011: an MLS and sonde derived ozone climatology for satellite retrieval algorithms. *J. Geophys. Res. Atmos.* 117 (D10), D10303 <https://doi.org/10.1029/2011JD017006>.
- Miyazaki, K., Bowman, K.W., Yumimoto, K., Walker, T., Sudo, K., 2020. Evaluation of a multi-model, multi-constituent assimilation framework for tropospheric chemical reanalysis. *Atmos. Chem. Phys.* 20 (2), 931–967. <https://doi.org/10.5194/acp-20-931-2020>.
- Miyazaki, K., Eskes, H.J., Sudo, K., Takigawa, M., van Weele, M., Boersma, K.F., 2012. Simultaneous assimilation of satellite NO<sub>2</sub>, O<sub>3</sub>, CO, and HNO<sub>3</sub> data for the analysis of tropospheric chemical composition and emissions. *Atmos. Chem. Phys.* 12 (20), 9545–9579. <https://doi.org/10.5194/acp-12-9545-2012>.
- Monks, P.S., Archibald, A.T., Colette, A., Cooper, O., Coyle, M., Derwent, R., et al., 2015. Tropospheric ozone and its precursors from the urban to the global scale from air quality to short-lived climate forcer. *Atmos. Chem. Phys.* 15 (15), 8889–8973. <https://doi.org/10.5194/acp-15-8889-2015>.
- Park, R.J., Jacob, D.J., Field, B.D., Yantosca, R.M., Chin, M., 2004. Natural and transboundary pollution influences on sulfate-nitrate-ammonium aerosols in the United States: implications for policy. *J. Geophys. Res. Atmos.* 109 (D15), D15204 <https://doi.org/10.1029/2003JD004473>.
- Parrington, M., Jones, D.B.A., Bowman, K.W., Horowitz, L.W., Thompson, A.M., Tarasick, D.W., Witte, J.C., 2008. Estimating the summertime tropospheric ozone distribution over North America through assimilation of observations from the Tropospheric Emission Spectrometer. *J. Geophys. Res. Atmos.* 113 (D18), D18307 <https://doi.org/10.1029/2007JD009341>.
- Parrington, M., Jones, D.B.A., Bowman, K.W., Thompson, A.M., Tarasick, D.W., Merrill, J., et al., 2009. Impact of the assimilation of ozone from the tropospheric emission spectrometer on surface ozone across north America. *Geophys. Res. Lett.* 36 (4), L04802 <https://doi.org/10.1029/2008GL036935>.
- Peng, Z., Lei, L., Liu, Z., Sun, J., Ding, A., Ban, J., et al., 2018. The impact of multi-species surface chemical observation assimilation on air quality forecasts in China. *Atmos. Chem. Phys.* 18, 17387–17404. <https://doi.org/10.5194/acp-18-17387-2018>.
- Quesada-Ruiz, S., Attié, J.L., Lahoz, W.A., Abida, R., Ricaud, P., El Amraoui, L., et al., 2020. Benefit of ozone observations from Sentinel-5P and future Sentinel-4 missions on tropospheric composition. *Atmos. Meas. Tech.* 13 (1), 131–152. <https://doi.org/10.5194/amt-13-131-2020>.
- Rodgers, C.D., 2000. *Inverse Methods for Atmospheric Sounding: Theory and Practice*. World Scientific.
- Shu, L., Wang, T., Han, H., Xie, M., Chen, P., Li, M., Wu, H., 2020. Summertime ozone pollution in the Yangtze River Delta of eastern China during 2013–2017: synoptic impacts and source apportionment. *Environ. Pollut.* 257, 113631 <https://doi.org/10.1016/j.envpol.2019.113631>.
- Shu, L., Xie, M., Wang, T., Gao, D., Chen, P., Han, Y., et al., 2016. Integrated studies of a regional ozone pollution synthetically affected by subtropical high and typhoon system in the Yangtze River Delta region, China. *Atmos. Chem. Phys.* 16 (24), 15801–15819. <https://doi.org/10.5194/acp-16-15801-2016>.
- Spurr, R.J.D., 2006. VLIDORT: a linearized pseudo-spherical vector discrete ordinate radiative transfer code for forward model and retrieval studies in multilayer multiple scattering media. *J. Quant. Spectrosc. Radiat. Transf.* 102 (2), 316–342. <https://doi.org/10.1016/j.jqsrt.2006.05.005>.
- Tang, X., Zhu, J., Wang, Z.F., Gbaguidi, A., 2011. Improvement of ozone forecast over Beijing based on ensemble Kalman filter with simultaneous adjustment of initial conditions and emissions. *Atmos. Chem. Phys.* 11, 12901–12916. <https://doi.org/10.5194/acp-11-12901-2011>.
- Timmermans, R.M.A., Lahoz, W.A., Attié, J.L., Peuch, V.H., Curier, R.L., Edwards, D.P., et al., 2015. Observing system simulation experiments for air quality. *Atmos. Environ.* 115, 199–213. <https://doi.org/10.1016/j.atmosenv.2015.05.032>.
- Veefkind, J.P., Aben, I., McMullan, K., Förster, H., de Vries, J., Otter, G., et al., 2012. TROPOMI on the ESA Sentinel-5 Precursor: a GMES mission for global observations of the atmospheric composition for climate, air quality and ozone layer applications. *Remote Sens. Environ.* 120, 70–83. <https://doi.org/10.1016/j.rse.2011.09.027>.
- Wiedinmyer, C., Akagi, S.K., Yokelson, R.J., Emmons, L.K., Al-Saadi, J.A., Orlando, J.J., Soja, A.J., 2011. The Fire Inventory from NCAR (FINN): a high resolution global model to estimate the emissions from open burning. *Geosci. Model Dev. (GMD)* 4 (3), 625–641. <https://doi.org/10.5194/gmd-4-625-2011>.
- Wu, L., Mallet, V., Bocquet, M., Sportisse, B., 2008. A comparison study of data assimilation algorithms for ozone forecasts. *J. Geophys. Res. Atmos.* 113 (D20), D20310 <https://doi.org/10.1029/2008JD009991>.
- Yadav, I.C., Linthoingambi Devi, N., Li, J., Syed, J.H., Zhang, G., Watanabe, H., 2017. Biomass burning in Indo-China peninsula and its impacts on regional air quality and global climate change-a review. *Environ. Pollut.* 227, 414–427. <https://doi.org/10.1016/j.envpol.2017.04.085>.
- Yeo, M.J., Kim, Y.P., 2021. Long-term trends of surface ozone in Korea. *J. Clean. Prod.* 294, 125352 <https://doi.org/10.1016/j.jclepro.2020.125352>.
- Yue, X., Unger, N., Harper, K., Xia, X., Liao, H., Zhu, T., et al., 2017. Ozone and haze pollution weakens net primary productivity in China. *Atmos. Chem. Phys.* 17 (9), 6073–6089. <https://doi.org/10.5194/acp-17-6073-2017>.
- Zaveri, R.A., Easter, R.C., Fast, J.D., Peters, L.K., 2008. Model for simulating aerosol interactions and chemistry (MOSAIC). *J. Geophys. Res. Atmos.* 113 (D13), D13204 <https://doi.org/10.1029/2007JD008782>.
- Zaveri, R.A., Peters, L.K., 1999. A new lumped structure photochemical mechanism for large-scale applications. *J. Geophys. Res. Atmos.* 104 (D23), 30387–30415. <https://doi.org/10.1029/1999JD900876>.
- Zheng, B., Tong, D., Li, M., Liu, F., Hong, C., Geng, G., et al., 2018. Trends in China's anthropogenic emissions since 2010 as the consequence of clean air actions. *Atmos. Chem. Phys.* 18 (19), 14095–14111. <https://doi.org/10.5194/acp-18-14095-2018>.
- Ziemke, J.R., Oman, L.D., Strode, S.A., Douglass, A.R., Olsen, M.A., McPeters, R.D., et al., 2019. Trends in global tropospheric ozone inferred from a composite record of TOMS/OMI/MLS/OMPS satellite measurements and the MERRA-2 GMI simulation. *Atmos. Chem. Phys.* 19 (5), 3257–3269. <https://doi.org/10.5194/acp-19-3257-2019>.
- Zoogman, P., Jacob, D.J., Chance, K., Liu, X., Lin, M., Fiore, A., Travis, K., 2014a. Monitoring high-ozone events in the US Intermountain West using TEMPO geostationary satellite observations. *Atmos. Chem. Phys.* 14 (12), 6261–6271. <https://doi.org/10.5194/acp-14-6261-2014>.
- Zoogman, P., Jacob, D.J., Chance, K., Worden, H.M., Edwards, D.P., Zhang, L., 2014b. Improved monitoring of surface ozone by joint assimilation of geostationary satellite observations of ozone and CO. *Atmos. Environ.* 84, 254–261. <https://doi.org/10.1016/j.atmosenv.2013.11.048>.
- Zoogman, P., Jacob, D.J., Chance, K., Zhang, L., Le Sager, P., Fiore, A.M., et al., 2011. Ozone air quality measurement requirements for a geostationary satellite mission. *Atmos. Environ.* 45 (39), 7143–7150. <https://doi.org/10.1016/j.atmosenv.2011.05.058>.
- Zoogman, P., Liu, X., Suleiman, R.M., Pennington, W.F., Flittner, D.E., Al-Saadi, J.A., et al., 2017. Tropospheric emissions: monitoring of pollution (TEMPO). *J. Quant. Spectrosc. Radiat. Transf.* 186, 17–39. <https://doi.org/10.1016/j.jqsrt.2016.05.008>.